Nanoscale

PAPER

View Article Online
View Journal | View Issue

Cite this: *Nanoscale*, 2024, **16**, 6259

Wurtzite *vs.* rock-salt MnSe epitaxy: electronic and altermagnetic properties†

Michał J. Grzybowski, *[a] Carmine Autieri, [b] Jaroslaw Domagala, [c] Cezary Krasucki,[a,c] Anna Kaleta, [c] Sławomir Kret, [c] Katarzyna Gas, [c,d] Maciej Sawicki, [c] Rafał Bożek, [a] Jan Suffczyński [a] and Wojciech Pacuski [a]

Newly discovered altermagnets are magnetic materials exhibiting both compensated magnetic order, similar to antiferromagnets, and simultaneous non-relativistic spin-splitting of the bands, akin to ferromagnets. This characteristic arises from specific symmetry operation that connects the spin sublattices. In this report, we show with *ab initio* calculations that semiconductive MnSe exhibits altermagnetic spin-splitting in the wurtzite phase as well as a critical temperature well above room temperature. It is the first material from such a space group identified to possess altermagnetic properties. Furthermore, we demonstrate experimentally through structural characterization techniques that it is possible to obtain thin films of both the intriguing wurtzite phase of MnSe and more common rock-salt MnSe using molecular beam epitaxy on GaAs substrates. The choice of buffer layers plays a crucial role in determining the resulting phase and consequently extends the array of materials available for the physics of altermagnetism.

Received 22nd September 2023,
Accepted 12th January 2024

DOI: 10.1039/d3nr04798a

rsc.li/nanoscale

I. Introduction

Intensive research on the physics of antiferromagnets in recent years led to the identification of materials that combine the properties of antiferromagnets (AFM) such as magnetization compensation together with the features of typical ferromagnets like spin-split band structures. Such coexistence of effects was shown to originate from the presence of rotation symmetry operation and the absence of translation symmetry operation connecting different spin sublattices in a generalized symmetry formalism and allowed for a definition of altermagnets,[1,2] which are distinct from both ferromagnets and antiferromagnets. Altermagnets are very appealing due to their potential applications, for example, they can exhibit outstanding charge–spin conversion efficiency[3–6] and large giant or tunneling magnetoresistance values[7] together with THz spin dynamics.[1] Numerous materials fulfill the symmetry criteria to be altermagnets ranging from insulators to metals.[1] Among them, hexagonal MnTe is an important chalcogenide semiconductor recently shown to exhibit an anomalous Hall effect.[8] This motivated us to search for altermagnetism in various crystal structures of manganese-based chalcogenides.

In this work, we investigate MnSe, which can form a variety of phases, although the most common form is the rock-salt structure. We show the possibility to stabilize the epitaxial growth of two different phases of thin film MnSe: rock-salt (RS) or wurtzite (WZ), depending on the appropriate choice of growth conditions with the use of the same MBE technique and GaAs substrates. During all of these processes, we observed sharp and bright reflection high-energy electron diffraction (RHEED) patterns as a sign of high-quality 2D growth. Of particular interest is the wurtzite phase that has been shown to be unstable in the bulk form[9] and thus rare. It was observed either as a minor impurity phase or in colloidal nanoparticles[10] but not for epitaxial thin films. We explore the structural properties and quality of thin films of MnSe by X-ray diffraction (XRD), transmission electron microscopy (TEM), energy-dispersive X-ray spectrometry (EDX), atomic force microscopy, Raman spectroscopy and superconducting quantum interference device (SQUID) magnetometry for the thicker layers of rock-salt MnSe.

Moreover, we performed *ab initio* calculations to explore the electronic band structure and found altermagnetic spin-splitting in the wurtzite MnSe together with the critical temperature above room temperature. The altermagnetism depends on the magnetic space groups, therefore, as a consequence, also

[a]*Faculty of Physics, University of Warsaw, ul. Pasteura 5, 02-093 Warsaw, Poland. E-mail: Michal.Grzybowski@fuw.edu.pl*
[b]*International Research Centre Magtop, Institute of Physics, Polish Academy of Sciences, Aleja Lotnikow 32/46, PL-02668 Warsaw, Poland*
[c]*Institute of Physics, Polish Academy of Sciences, Aleja Lotnikow 32/46, PL-02668 Warsaw, Poland*
[d]*Center for Science and Innovation in Spintronics, Tohoku University, Sendai 980-8577, Japan*

† Electronic supplementary information (ESI) available. See DOI: https://doi.org/10.1039/d3nr04798a

on the Wyckoff positions of the magnetic atoms, magnetic order and dimensionality.[1,11,12] Several compounds belonging to the hexagonal space group no. 194 (NiAs phase) show altermagnetism as MnTe and $EuIn_2As_2$ compounds.[1,8,13] Going to the hexagonal space group no. 186 (wurtzite phase), MnSe is the first altermagnetic compound proposed within this space group to our knowledge.

Historically, the interplay of different phases has been observed very early for bulk MnSe. Although the most thermodynamically stable form of MnSe is the rock-salt structure MnSe,[14,15] different crystalline phases were believed to transform between each other upon cooling and heating cycles, which was considered as a likely reason for the strong thermal hysteretic behavior of its magnetic properties.[16] Alternative explanations have been provided[17] but more recent research proves the existence of an admixture of hexagonal NiAs-type MnSe at lower temperatures[18,19] and correlates it with the existence of the hysteresis. Remarkably, high pressure may induce a transformation to the orthogonal phase and superconductivity.[20,21] The epitaxial growth of MnSe on (100) GaAs is known to result in a rock-salt structure[22] except for very thin layers.[22–24] Successful efforts of stabilizing the zinc blende structure in the MBE were undertaken by the growth of superlattices with ZnSe on (100) GaAs.[23,25,26] The growth of MnSe on *c*-plane sapphire[27] or $NbSe_2$[28] substrates has also been attempted. The latter can result in a monolayer of unusual ordering. Computations confirm that the choice of the substrate and the resulting strain can have a tremendous effect on the magnetic properties of this material.[29]

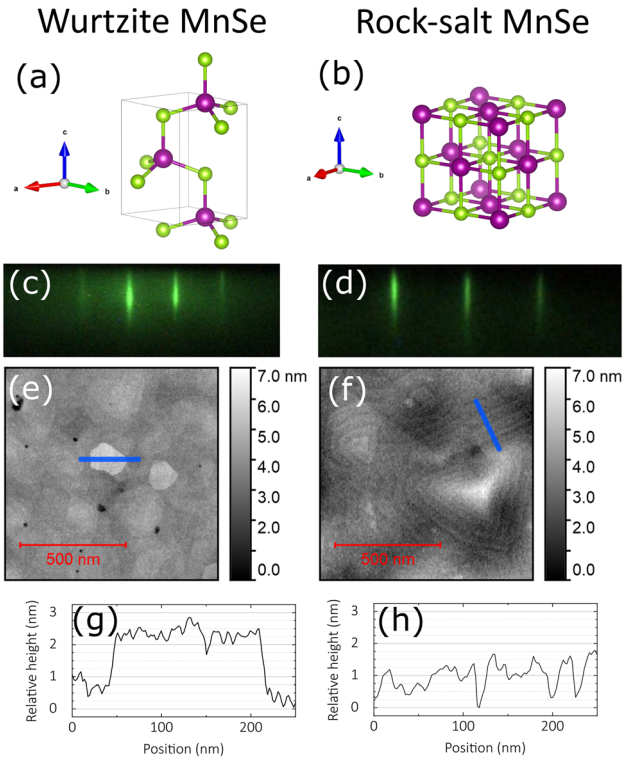

Fig. 1 Comparison of the structural characteristics of the top surface of wurtzite MnSe (left column, sample WZ3) and rock-salt MnSe (right column, sample RS1). Atomic structure diagrams of (a) wurtzite and (b) rock-salt MnSe. (c) and (d) RHEED images taken just at the end of the growth. (e) and (f) AFM topography scans and (g) and (h) profiles of the relative height along the blue lines indicated in the AFM images.

II. Experimental results and discussion

A. Rock-salt MnSe

All MnSe layers considered in this work were grown in a II–VI MBE growth chamber equipped with standard Knudsen effusion cells for both Se and Mn sources. We start from the general notice that the growth of MnSe directly on GaAs without any buffer layers results in a rock-salt structure of the former (see Fig. 1b). For GaAs(100) with 2° offcut substrates, the RHEED image gradually transforms from the 2D streaky to a 3D spotted pattern. The change of the distance between the lines is a sign of diminishing lattice constant can be observed. Significant lattice mismatch is expected to promote the formation of defects. The crystal structure quality was studied by XRD and reflections corresponding to the (002), (004) and (006) planes of rock-salt MnSe could be observed in $2\theta/\omega$ scans. The width of the (004) reflection was studied as a function of the temperature of growth. Although a slightly narrower peak has been observed for a temperature of T = 350 °C, we chose the temperature of T = 300 °C as optimal for the growth of all samples considered in this work. This is because elevated temperatures preclude the growth of numerous II–VI buffer layers.

In contrast to other works considering the growth of MnSe by the MBE,[22–26] we also attempted the use of GaAs substrates with (111)B orientation. Remarkably, such a procedure results in a 2D RHEED pattern that remains in the form of bright and sharp lines up to a thickness of hundreds of nanometers (Fig. 1d). The surface of the 200 nm layer of MnSe (sample RS1) studied by atomic force microscopy (Fig. 1f) exhibits subnanometer roughness measured over hundreds of nanometers (Fig. 1h), the presence of terraces of a triangular shape, screw dislocation patterns and occasional large surface defects of a round shape. The RMS roughness parameter calculated for a random 500 nm square region is on the order of 0.6 nm. In the XRD patterns, reflections corresponding to the (111) and (222) rock-salt phases of MnSe are clearly visible in the $2\theta/\omega$ scans (blue line in Fig. 2). We observed an almost fully relaxed unit cell (ESI†). Moreover, the sample exhibits a 6-fold symmetry with respect to the ⟨111⟩ plane unlike the GaAs substrate, which displays a 3-fold symmetry (ESI†). It is most likely the sign of crystal twinning that arises due to the high symmetry of the plane during the growth and 0° substrate offcut. It can be likely mitigated with the use of substrates with significant offcut with respect to the (111) plane.

Magnetic measurements of the rock-salt RS1 sample were performed using a SQUID-based magnetometer MPMS XL

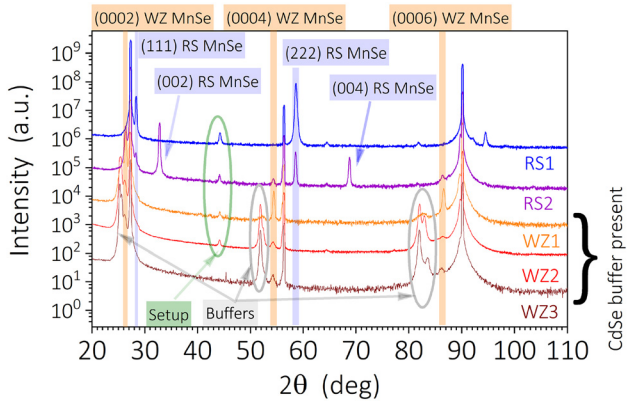

Fig. 2 Comparison of $2\theta/\omega$ scans for structures with top MnSe(111) thin-film layers evidencing an emergence of the wurtzite phase when CdSe buffer is present.

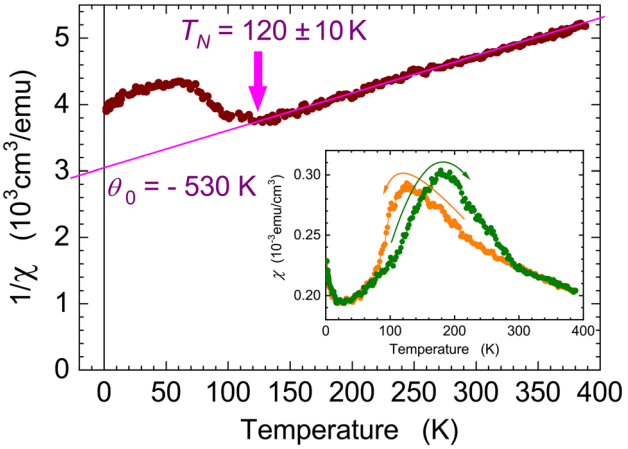

Fig. 3 Inverse of the magnetic susceptibility, χ, of rock-salt MnSe (sample RS1) established at $\mu_0 H$ = 4 T (solid symbols). The solid line represents the Curie–Weiss behavior allowing for the estimation of the Curie–Weiss temperature Θ_{CW} = −530 ± 30 K and the magnitude of spin moment S = 2.4 ± 0.2. The thick arrow marks the Néel temperature T_N of this compound. Inset: thermal hysteresis of χ, characteristic of rock-salt MnSe, evidenced at an external field of $\mu_0 H$ = 1 T.

from Quantum Design (San Diego, CA, USA). We followed strictly the code appropriate for measurements for thin magnetic layers of minute magnetic signals deposited on solid-state bulky substrates.[30] The sample was stabilized with the help of a strongly ethanol-diluted GE varnish on a sample holder made from a length of about 1.8 mm of a wide Si stick. To correctly establish the signal specific to the thin MnSe layer, reference measurements were performed at the same temperature and magnetic field ranges for an otherwise identical piece of the GaAs substrate mounted in a similar manner on the same sample holder. This extra effort is especially important since commercial solid-state substrates exhibit a sizable temperature-dependent response,[31,32] which can be easily comparable to that of the investigated layers, in particular, antiferromagnets, and so it needs to be subtracted accordingly with adequate care. The results of our T-dependent studies are summarized in Fig. 3. In accordance with the finding of ref. 18, strong thermal hystereses are seen between 70 and 300 K, as exemplified in the inset of Fig. 3. The magnitudes of these anomalies (in comparison with the magnetic susceptibility $\chi(T)$ at T > 300 K) decrease substantially at stronger magnetic fields H. So, in order to establish the Néel temperature T_N of rock-salt MnSe, we limit our analysis here to the results obtained at relatively high magnetic fields. The inverse of $\chi(T)$ established for $\mu_0 H$ = 4 T is given in the main panel of Fig. 3. It follows a sufficiently straight line at elevated temperatures to allow us to apply the time-honored Curie–Weiss (CW) approach. The abscissa and slope of this line yield the estimation of the Curie–Weiss temperature Θ_{CW} = −530 ± 30 K and the magnitude of spin moment S = 2.4 ± 0.2, respectively. The latter value confirms the expected $3d^5$ configuration of Mn ions in rock-salt MnSe. The experimental points follow the CW law only above about 120 K. Below this temperature, the experimental points clearly deviate from the linear dependency. We assigned this temperature to T_N = 120 ± 10 K of rock-salt MnSe. We marked this point by a thick arrow in Fig. 3. This is the magnitude of T_N as established previously from heat capacity measurements.[18]

For Raman spectroscopy measurements, the rock-salt MnSe sample (RS3) was placed in a helium flow cryostat. The Raman spectra were recorded with the use of a 532 nm laser and the signal were collected with a microscope objective of a numerical aperture of NA = 0.65. Fig. 4a shows the Raman scattering spectrum of the material recorded at 75 K. Transitions at around 130 cm^{-1} and 277 cm^{-1}, characteristic of rock-salt MnSe,[33] are clearly observed. Fig. 4b shows the Raman spectra in the spectral vicinity of the transition at around 130 cm^{-1} recorded for consecutive temperatures increasing from 70 K to 170 K. The transition is attributed to the excitation of the LA (X) phonon in rock-salt MnSe.[33] The intensity of the transition is presented in Fig. 4c. It exhibits a minimum at around 120 K, corresponding to the Néel temperature in this material. A decrease in the Raman transition intensity was observed at around T_N, which confirms that phonon excitation provides a probe for the magnetic phase transitions in the studied system. This can be traced back to a contribution of an exchange type apart from the ordinary Coulomb-type interaction between the Mn cations possessing non-vanishing spin moment. Similar effects have been previously observed mostly in 2D layered AFMs, where phonon interactions are much stronger.[34]

Next, we describe the growth of MnSe on the buffer layers deposited on GaAs(111)B (see the full list of the investigated samples in Table 1). One of the commonly used buffers for II–VI semiconductors is ZnSe. However, for the growth of ZnSe in the (111) orientation, the RHEED pattern evolves into a spotty 3D image precluding the growth of thick layers of high quality. For a 60 nm ZnSe buffer, the subsequent layer of MnSe (sample RS2) exhibits rock-salt character but with a mixture of ⟨111⟩ and ⟨001⟩ orientations and a likely admixture of the wurtzite phase (purple line in Fig. 2).

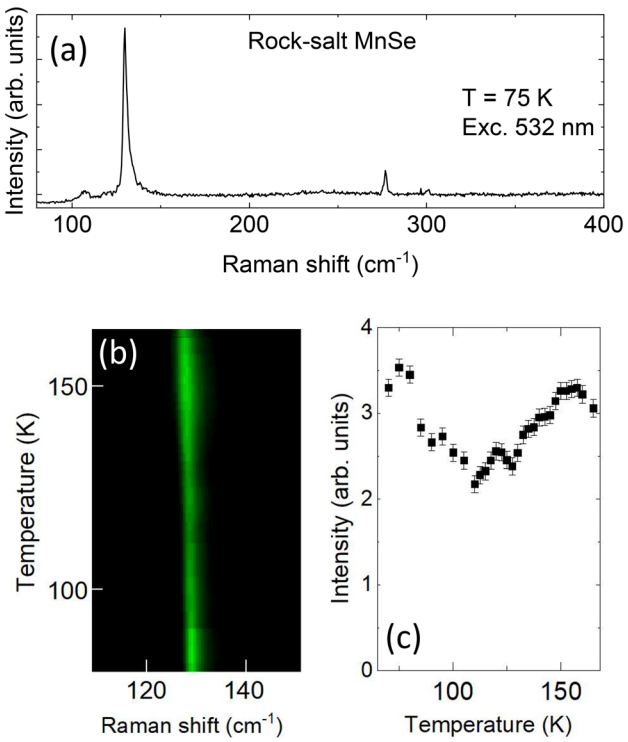

Fig. 4 (a) Raman scattering spectrum of the rock-salt MnSe layer (sample RS3) recorded at 75 K. (b) Raman spectra of the rock-salt MnSe layer (sample RS3) as a function of temperature in the region of 130 cm^{-1} transition. (c) Intensity of the transition at around 130 cm^{-1} as a function of temperature exhibits a clear minimum in the vicinity of the Néel temperature.

Table 1 The list of investigated MBE-grown samples containing rock-salt (RS) or wurtzite (WZ) MnSe as a top layer. All of the listed samples were grown on GaAs(111)B substrates

Sample number	Sample structure (thickness in nm)	Phase of MnSe
RS1 (UW1932)	**MnSe (200)**	RS
RS2 (UW1933)	ZnSe (60)|**MnSe (200)**	RS/WZ
RS3 (UW2097)	**MnSe (2500)**	RS
WZ1 (UW1947)	ZnSe (60)|CdSe (10)|**MnSe (60)**	WZ
WZ2 (UW1961)	ZnSe (70)|ZnTe (50)|(Cd,Mg)Se (50)|CdSe (10)|**MnSe (20)**	WZ
WZ3 (UW1994)	ZnSe (70)|ZnTe (50)|(Cd,Mg)Se (50)|CdSe (20)|**MnSe (20)**	WZ

B. Wurtzite MnSe

CdSe can be grown on GaAs(111) in the wurtzite phase[35–37] (see Fig. 1a). This holds true even if additional layers of ZnSe|ZnTe are introduced in between (Fig. 5). Remarkably, we observed that for every sample in our study in which the MnSe layer is grown on CdSe, MnSe adopts the wurtzite phase (see the list of the studied samples in Table 1). This is verified by XRD and TEM. The reflections corresponding to the (0002), (0004) and (0006) wurtzite phases of MnSe can be seen in Fig. 2. Due to the thin film character of the wurtzite MnSe layers (unlike rock-salt MnSe, we discuss the thickness limitations in the ESI†), we focus on the detailed TEM analysis for this phase rather than bulk-sensitive techniques that are difficult to apply here such as Raman spectroscopy and SQUID magnetometry.

The (scanning) transmission electron microscopy analysis in Fig. 5 shows the results for the cross-section of the WZ2 sample (prepared with a focused ion beam), revealing its chemical composition (Fig. 5a) and a detailed analysis of the crystal structure of the MnSe layer in Fig. 5b–d. The color-coded energy-dispersive X-ray spectroscopy (EDX) maps in Fig. 5a confirm that the heterostructure outcome is in accordance with MBE specifications (see Table 1). Comprehensive structural studies on MnSe phase identification were performed *via* high-resolution TEM (HRTEM) imaging in correlation with fast Fourier transform (FFT) analysis (electron diffraction analog), which unequivocally confirms the wurtzite phase of MnSe. Clear evidence is presented in Fig. 5c that a wurtzite MnSe ball model (in the $[2\bar{1}\bar{1}0]$ zone axis) is superimposed on the HRTEM image in its thinnest area (top part) as well in Fig. 5d, where the simulated kinematic electron diffraction pattern aligns with the FFT image.

The RHEED pattern of the surface of wurtzite MnSe consists of sharp and bright lines throughout the growth of the layers of at least 60 nm thickness (Fig. 1c). The surface measured by AFM is subnanometer flat over hundreds of nm distances as indicated in Fig. 1e and g and the RMS roughness parameter calculated for a random 500 nm square region is on the order of 1.5 nm.

The complex set of buffer layers beneath wurtzite CdSe, introduced for some of the studied samples, was motivated by analogous experimental protocols that had been developed and successfully tested for high-quality CdSe quantum wells grown on GaAs(001)-oriented substrates.[38,39] Therefore, we noticed that some of our samples should form an interesting asymmetric quantum well that can be studied optically. The limitations of the quality of ZnSe growth in the (111) orientation and the simultaneous good quality RHEED pattern for CdSe in the same samples together with the universal observation of wurtzite MnSe on CdSe within the studied set of samples suggest that the crucial factor to obtain wurtzite MnSe is to proceed deposition on wurtzite CdSe.

III. First principles calculations

Electronic structure calculations were performed within the framework of first-principles density functional theory based on the plane wave basis set and the projector augmented wave method using VASP[40] package. A plane-wave energy cut-off of 400 eV and the generalised gradient approximation of Perdrew, Burke, and Ernzerhof have been used.[41] We have performed the calculations using 10 × 10 × 6 *k*-points centered in Γ. The Hubbard U effects for the 3d-orbitals of Mn^{2+} have been

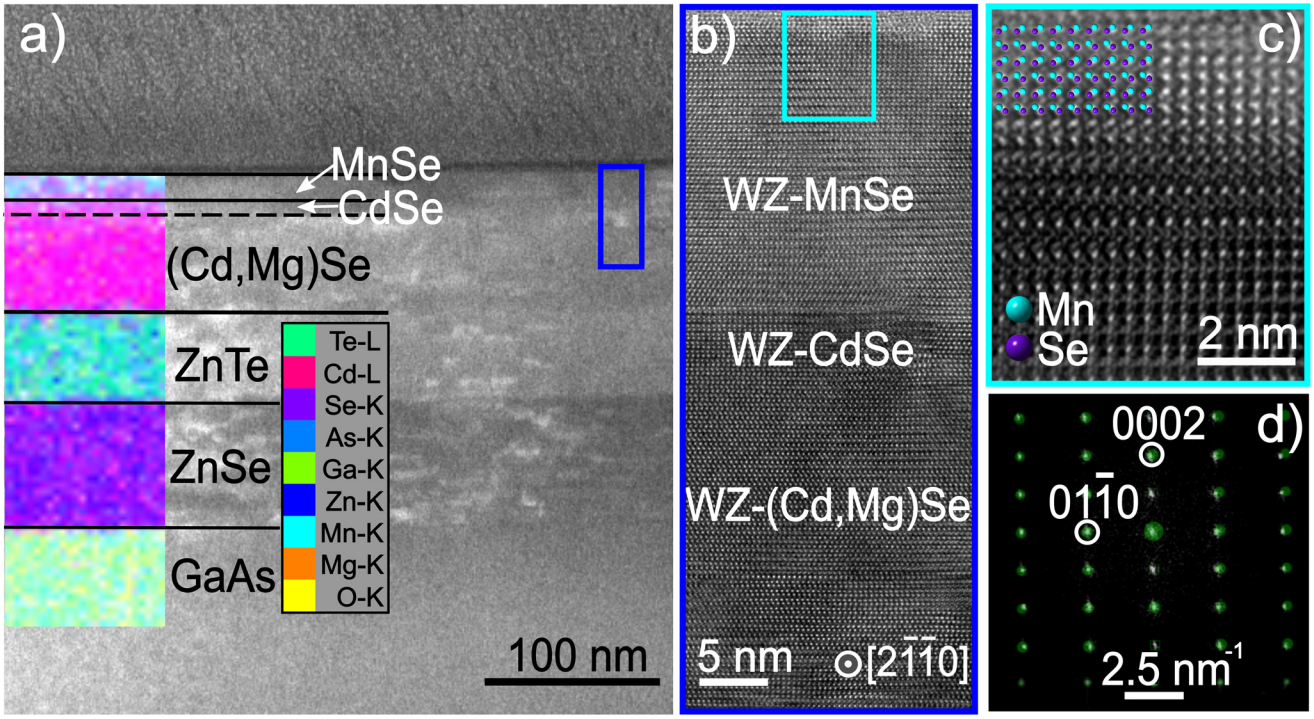

Fig. 5 (a) Scanning transmission electron microscopy (STEM) image of a sample containing wurtzite MnSe (sample WZ2); cross-section with energy-dispersive X-ray spectroscopy (EDX) color maps showing the GaAs substrate and ZnSe and ZnTe buffer layers, as well as (Cd,Mg)Se, CdSe, MnSe top layers; (b) high-resolution TEM (HRTEM) image of the dark blue rectangle area indicated in panel a, presenting wurtzite MnSe and wurtzite CdSe/(Cd,Mg)Se layers in a perfect epitaxial relationship recorded in the [2$\bar{1}\bar{1}$0] zone axis. (c) Magnified area from panel b (light blue rectangle) with an atom-ball model of the wurtzite MnSe structure (visualized in the [2$\bar{1}\bar{1}$0] zone axis) superimposed on the HRTEM image. (d) Kinematic electron diffraction simulated for wurtzite MnSe (green spots) perfectly overlapping the 2D-fast Fourier transform (FFT) of the image in panel c (grayscale image in the background).

adopted.[42] We have scanned the value of U from 0 to 6 eV (ref. 43 and 44) keeping $J_H = 0.15U$. Using first-principles calculations, we compared the rock-salt crystal structure (space group no. 225) with the wurtzite crystal structure (space group no. 186). The band gap changes from indirect in the rock-salt phase[45] to direct in the wurtzite phase as we can see in Fig. 6a and b. In the wurtzite phase, the valence band is composed of p-Se from −4 eV up to the Fermi level. The majority-spin d-bands are quite flat and present in between −5 and −6 eV as observed in (Cd,Mn)Te.[46] At the Γ point, the bottom of the conduction is composed of s bands of Te and Mn. We investigated the band gap E_g as a function of the Coulomb repulsion U in Fig. 6c. As usual, the band gap increases monotonically as a function of U for both cases and we found that the band gap of the wurtzite phase is always 1.5 eV larger than the rock-salt phase. We recall that *ab initio* calculations tend to underestimate the gap; this underestimation is particularly severe in the wurtzite phase as we can see from ZnO calculations.[47] However, we expect that the prediction of the difference between the gaps would be much more reliable; therefore, we expect that the wurtzite band gap is around 1.5 eV larger than the rock-salt phase band gap.

To investigate the magnetic properties, we analyzed the quantity $\Delta E = E_{FM} - E_{AFM}$ per formula unit as a function of U for both rock-salt and wurtzite phases. The quantity ΔE is proportional to the magnetic exchange and therefore to T_N. As we can see from Fig. 6d, in both cases, the AFM phase is the ground state. However, in the rock-salt phase, AFM is magnetically frustrated, producing a relatively low value of ΔE while the energy difference is much larger for the wurtzite phase. Considering that the rock-salt phase has T_N = 120 K detected experimentally, the wurtzite MnSe has T_N well above room temperature. From *ab initio* calculations, the Néel vector is in the *ab* plane with a small energy difference between the magnetic configurations with spins in the plane and out of the plane. The magnetocrystalline anisotropy is of the order of 0.02–0.06 eV per formula unit for values of the Coulomb repulsion U in the physical range of U between 2 and 6 eV.

Regarding the altermagnetism, the rock-salt phase is not altermagnetic since both magnetic and non-magnetic atoms are in high-symmetry positions. The altermagnetic properties are present in the wurtzite phase of MnSe since the two Mn sites with opposite magneticmoments can be transformed one into another only by combining a non-primitive translation with a rotation by 60 degrees around the *c*-axis due to the presence of non-magnetic Se atoms. The non-relativistic spin-splitting is similar to the NiAs phase except that the splitting is much smaller in the wurtzite MnSe. Indeed, both groups belong to the same magnetic Laue class (6′/m′m′m), proving that the spin splitting of electron bands without spin–orbit

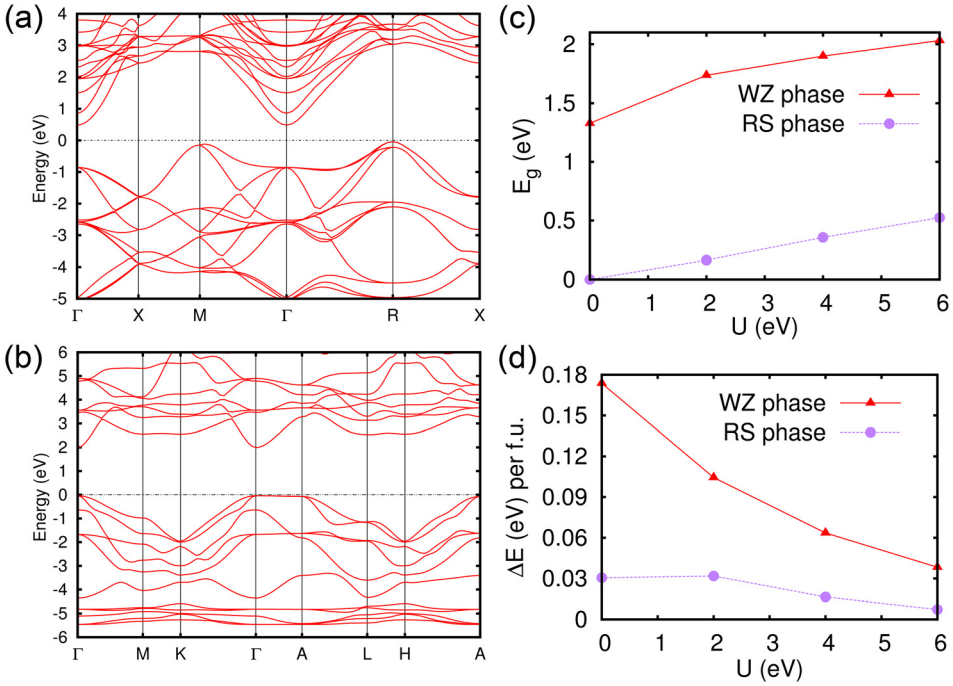

Fig. 6 (a) Magnetic band structure of MnSe in the rock-salt phase (space group no. 225). (b) Magnetic band structure of MnSe in the wurtzite phase (space group no. 186). The Fermi level is set to zero. In both cases, we have used a value of U = 6 eV. (c) Band gap of the rock-salt phase (purple line) and wurtzite phase (red line) as a function of the Coulomb repulsion U. (d) Energy difference per formula unit for the rock-salt phase (purple line) and wurtzite phase (red line) as a function of the Coulomb repulsion. The deviation from the trend for the rock-salt phase at low U is due to the insulator-to-metal transition of the FM phase at U = 0.

coupling is qualitatively the same in both systems. However, the magnetic point group of the wurtzite MnSe is 6′m′m, which differs from that of the hexagonal MnTe in the NiAs structure, which is 6′/m′m′m.[48,49] Therefore, the spin–orbit effects on the band structure differ between thecentrosymmetric MnTe and noncentrosymmetric MnSe as it was demonstrated elsewhere.[50] The band structure along the k-path that shows altermagnetism is presented in Fig. 7. With subscripts 1 and 2 in Fig. 7, we indicate the two points in the k-space that have opposite non-relativistic spin-splitting. The points L_1 and L_2 have the same position of the Brillouin zone as it is in the case of MnTe.[51]

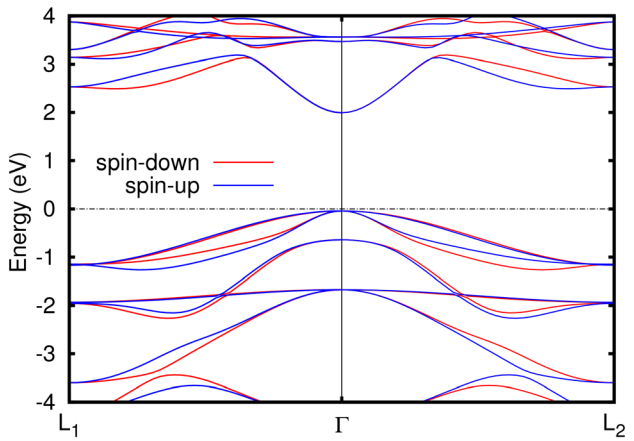

Fig. 7 Magnetic band structure of wurtzite MnSe along the high-symmetry positions L_1-Γ-L_2 in the absence of SOC. Blue and red lines represent the spin-up and spin-down channels, respectively. The Fermi level is set to zero. Altermagnetism is revealed by the lifted degeneracy of the spin-up and spin-down channels.

IV. Conclusions

In summary, we report on the MBE growth and structural studies of the thin layers of the semiconductor MnSe in the (111) orientation for the first time. We revealed the possibility of controlling the crystal structure of the resulting MnSe. The growth directly on GaAs substrates leads to the typical rock-salt structure of MnSe, whereas the presence of a wurtzite CdSe buffer layer underneath makes MnSe adopt the wurtzite structure, which is a rare phase for this compound. With *ab initio* calculations, we have demonstrated that the wurtzite MnSe is an altermagnetic compound with lower non-relativistic spin-splitting with respect to the NiAs phase of MnTe. Moreover, the calculations show that wurtzite MnSe has a direct band gap of 1.5 eV larger than the rock-salt phase of MnSe and a Néel temperature above room temperature. Such interesting observations extend the array of materials available for the physics of altermagnetism and highlight the role of the proper choice of the buffer layers in the epitaxial growth of manganese-based chalcogenides.

Conflicts of interest

There are no conflicts to declare.

Acknowledgements

This research was funded by the National Science Centre, Poland 2021/40/C/ST3/00168. C. A. was supported by the Foundation for Polish Science through the International Research Agendas program co-financed by the European Union within the Smart Growth Operational Programme (grant no. MAB/2017/1). C. A. acknowledges the access to the computing facilities of the Interdisciplinary Center of Modeling at the University of Warsaw, grant g91-1418, g91-1419 and g91-1426 for the availability of high-performance computing resources and support. C. A. acknowledges the CINECA award under the ISCRA initiative IsC99 "SILENTS", IsC105 "SILENTSG" and IsB26 "SHINY" grants for the availability of high-performance computing resources and support. C. A. acknowledges the access to the computing facilities of the Poznan Supercomputing and Networking Center grant no. 609. J. S. acknowledges the support within the "New Ideas 2B in POB II" IDUB project financed by the University of Warsaw. Atomic structure diagrams were prepared with VESTA software.[52] We would like to thank dr Mateusz Tokarczyk for complementary XRD measurements.

References

1 L. Šmejkal, J. Sinova and T. Jungwirth, Emerging Research Landscape of Altermagnetism, *Phys. Rev. X*, 2022, **12**, 040501.
2 L. Šmejkal, J. Sinova and T. Jungwirth, Beyond Conventional Ferromagnetism and Antiferromagnetism: A Phase with Nonrelativistic Spin and Crystal Rotation Symmetry, *Phys. Rev. X*, 2022, **12**, 031042.
3 R. González-Hernández, L. Šmejkal, K. Výborný, Y. Yahagi, J. Sinova, T. Jungwirth and J. Železný, Efficient Electrical Spin Splitter Based on Nonrelativistic Collinear Antiferromagnetism, *Phys. Rev. Lett.*, 2021, **126**, 127701.
4 A. Bose, N. J. Schreiber, R. Jain, D.-F. Shao, H. P. Nair, J. Sun, X. S. Zhang, D. A. Muller, E. Y. Tsymbal, D. G. Schlom and D. C. Ralph, Tilted spin current generated by the collinear antiferromagnet ruthenium dioxide, *Nat. Electron.*, 2022, **5**, 267–274.
5 H. Bai, L. Han, X. Y. Feng, Y. J. Zhou, R. X. Su, Q. Wang, L. Y. Liao, W. X. Zhu, X. Z. Chen, F. Pan, X. L. Fan and C. Song, Observation of Spin Splitting Torque in a Collinear Antiferromagnet RuO_2, *Phys. Rev. Lett.*, 2022, **128**, 197202.
6 S. Karube, T. Tanaka, D. Sugawara, N. Kadoguchi, M. Kohda and J. Nitta, Observation of Spin-Splitter Torque in Collinear Antiferromagnetic RuO_2, *Phys. Rev. Lett.*, 2022, **129**, 137201.
7 L. Šmejkal, A. B. Hellenes, R. González-Hernández, J. Sinova and T. Jungwirth, Giant and Tunneling Magnetoresistance in Unconventional Collinear Antiferromagnets with Nonrelativistic Spin-Momentum Coupling, *Phys. Rev. X*, 2022, **12**, 011028.
8 R. D. Gonzalez Betancourt, J. Zubáč, R. Gonzalez-Hernandez, K. Geishendorf, Z. Šobáň, G. Springholz, K. Olejník, L. Šmejkal, J. Sinova, T. Jungwirth, S. T. B. Goennenwein, A. Thomas, H. Reichlová, J. Železný and D. Kriegner, Spontaneous Anomalous Hall Effect Arising from an Unconventional Compensated Magnetic Phase in a Semiconductor, *Phys. Rev. Lett.*, 2023, **130**, 036702.
9 A. Baroni, Sul polimorfismo di MnSe, *Z. Kristallogr. – Cryst. Mater.*, 1938, 336.
10 I. T. Sines, R. Misra, P. Schiffer and R. E. Schaak, Colloidal Synthesis of Non-Equilibrium Wurtzite-Type MnSe, *Angew. Chem., Int. Ed.*, 2010, **49**, 4638–4640.
11 G. Cuono, R. M. Sattigeri, J. Skolimowski and C. Autieri, Orbital-selective altermagnetism and correlation-enhanced spin-splitting in strongly-correlated transition metal oxides, *J. Magn. Magn. Mater.*, 2023, **586**, 171163.
12 A. Fakhredine, R. M. Sattigeri, G. Cuono and C. Autieri, Interplay between altermagnetism and nonsymmorphic symmetries generating large anomalous Hall conductivity by semi-Dirac points induced anticrossings, *Phys. Rev. B*, 2023, **108**, 115138.
13 G. Cuono, R. M. Sattigeri, C. Autieri and T. Dietl, Ab initio overestimation of the topological region in Eu-based compounds, *Phys. Rev. B*, 2023, **108**, 075150.
14 M. E. Schlesinger, The Mn-Se (manganese-selenium) system, *J. Phase Equilib.*, 1998, **19**, 588–590.
15 N. Li, L. Zhu, H. Shang, F. Wang, Y. Zhang, Y. Yao, J. Wang, X. Zhan, F. Wang, J. He and Z. Wang, Controlled synthesis and Raman study of a 2D antiferromagnetic P-type semiconductor: α-MnSe, *Nanoscale*, 2021, **13**, 6953–6964.
16 R. Lindsay, Magnetic Susceptibility of Manganese Selenide, *Phys. Rev.*, 1951, **84**, 569–571.
17 T. Ito, K. Ito and M. Oka, Magnetic Susceptibility, Thermal Expansion and Electrical Resistivity of MnSe, *Jpn. J. Appl. Phys.*, 1978, **17**, 371–374.
18 C.-H. Huang, C.-W. Wang, C.-C. Chang, Y.-C. Lee, G.-T. Huang, M.-J. Wang and M.-K. Wu, Anomalous magnetic properties in Mn(Se, S) system, *J. Magn. Magn. Mater.*, 2019, **483**, 205–211.
19 J. B. C. Efrem D'Sa, P. A. Bhobe, K. R. Priolkhar, A. Das, P. S. R. Krishna, P. R. Sarode and R. B. Prabhu, Low Temperature Magnetic Structure of MnSe, *Pramana*, 2004, **63**, 227–232.
20 T. L. Hung, C. H. Huang, L. Z. Deng, M. N. Ou, Y. Y. Chen, M. K. Wu, S. Y. Huyan, C. W. Chu, P. J. Chen and T. K. Lee, Pressure induced superconductivity in MnSe, *Nat. Commun.*, 2021, **12**, 5436.

21 X.-X. Man, B.-C. Gong, P.-H. Sun, K. Liu and Z.-Y. Lu, First-principles study on the magnetic and electronic properties of the high-pressure orthorhombic phase of MnSe, *Phys. Rev. B*, 2022, **106**, 035136.
22 H. Kim, R. Vogelgesang, A. K. Ramdas, F. C. Peiris, U. Bindley and J. K. Furdyna, MnSe: Rocksalt versus zinc-blende structure, *Phys. Rev. B: Condens. Matter Mater. Phys.*, 1998, **58**, 6700–6703.
23 W. Heimbrodt, O. Goede, I. Tschentscher, V. Weinhold, A. Klimakow, U. Pohl, K. Jacobs and N. Hoffmann, Optical study of octahedrally and tetrahedrally coordinated MnSe, *Phys. B*, 1993, **185**, 357–361.
24 S. Chang, D. Lee, H. Nakata, A. V. Nurmikko, L. A. Kolodziejski and R. L. Gunshor, Frustrated antiferromagnetism at heterointerfaces in a semiconductor superlattice: MnSe/ZnSe, *J. Appl. Phys.*, 1987, **62**, 4835–4838.
25 L. A. Kolodziejski, R. L. Gunshor, N. Otsuka, B. P. Gu, Y. Hefetz and A. V. Nurmikko, Two-dimensional metastable magnetic semiconductor structures, *Appl. Phys. Lett.*, 1986, **48**, 1482–1484.
26 I. Ishibe, Y. Nabetani, T. Kato and T. Matsumoto, MBE growth of MnSe/ZnSe superlattices on GaAs (1 0 0) vicinal substrates, *J. Cryst. Growth*, 2000, **214–215**, 172–177.
27 J. Kucharek, R. Bożek and W. Pacuski, MnSe - Molecular Beam Epitaxy Growth and Optical Characterisation, *Acta Phys. Pol., A*, 2019, **136**, 598–602.
28 M. Aapro, M. N. Huda, J. Karthikeyan, S. Kezilebieke, S. C. Ganguli, H. G. Herrero, X. Huang, P. Liljeroth and H. P. Komsa, Synthesis and Properties of Monolayer MnSe with Unusual Atomic Structure and Antiferromagnetic Ordering, *ACS Nano*, 2021, **15**, 13794–13802.
29 K. Nakamura, T. Akiyama, T. Ito and A. J. Freeman, Magnetic structures and half-metallicity at zincblende ferromagnetic/antiferromagnetic interfaces: Role of tetragonal distortions, *J. Magn. Magn. Mater.*, 2007, **310**, 2186–2188.
30 M. Sawicki, W. Stefanowicz and A. Ney, Sensitive SQUID magnetometry for studying nanomagnetism, *Semicond. Sci. Technol.*, 2011, **26**, 064006.
31 A. Ney, J. S. Harris and S. S. Parkin, Temperature dependent magnetic properties of the GaAs substrate of spin-LEDs, *J. Phys.: Condens.Matter*, 2006, **18**, 4397–4406.
32 K. Gas and M. Sawicki, A Simplified Method of the Assessment of Magnetic Anisotropy of Commonly Used Sapphire Substrates in SQUID Magnetometers, *Materials*, 2022, **15**, 8532.
33 Z. V. Popović and A. Milutinović, Far-infrared reflectivity and Raman scattering study of α-MnSe, *Phys. Rev. B: Condens. Matter Mater. Phys.*, 2006, **73**, 155203.
34 D. Vaclavkova, A. Delhomme, C. Faugeras, M. Potemski, A. Bogucki, J. Suffczyński, P. Kossacki, A. R. Wildes, B. Grémaud and A. Saúl, Magnetoelastic interaction in the two-dimensional magnetic material MnPS 3 studied by first principles calculations and Raman experiments, *2D Mater.*, 2020, **7**, 035030.
35 M. Grün, M. Hetterich, U. Becker, H. Giessen and C. Klingshirn, Wurtzite-type CdS and CdSe epitaxial layers I. Growth and characterization, *J. Cryst. Growth*, 1994, **141**, 68–74.
36 M. Göppert, M. Hetterich, A. Dinger, C. Klingshirn and K. P. O'Donnell, Infrared spectroscopy of confined optical and folded acoustical phonons in strained CdSe/CdS superlattices, *Phys. Rev. B: Condens. Matter Mater. Phys.*, 1998, **57**, 13068–13071.
37 N. Matsumura, J. Ueda and J. Saraie, Molecular beam epitaxial growth of hexagonal CdSe and ZnCdSe on cubic GaAs(111)B substrates, *Jpn. J. Appl. Phys.*, 2000, **39**, 1026–1028.
38 K. Sawicki, J.-G. Rousset, R. Rudniewski, W. Pacuski, M. Ściesiek, T. Kazimierczuk, K. Sobczak, J. Borysiuk, M. Nawrocki and J. Suffczyński, Triple threshold lasing from a photonic trap in a Te/Se-based optical microcavity, *Commun. Phys.*, 2019, **2**, 38.
39 K. Sawicki, M. Jurczak, W. Pacuski and J. Suffczyński, Direct Interbranch Relaxation of Polaritons in a Microcavity with Embedded CdSe/(Cd,Mg)Se Quantum Wells, *J. Electron. Mater.*, 2020, **49**, 4531–4536.
40 G. Kresse and J. Furthmüller, Efficient iterative schemes for ab initio total-energy calculations using a plane-wave basis set, *Phys. Rev. B: Condens. Matter Mater. Phys.*, 1996, **54**, 11169.
41 J. P. Perdew, K. Burke and M. Ernzerhof, Generalized gradient approximation made simple, *Phys. Rev. Lett.*, 1996, **77**, 3865.
42 A. I. Liechtenstein, V. I. Anisimov and J. Zaanen, Density-functional theory and strong interactions: Orbital ordering in Mott-Hubbard insulators, *Phys. Rev. B: Condens. Matter Mater. Phys.*, 1995, **52**, R5467–R5470.
43 S. A. Ivanov, A. A. Bush, A. I. Stash, K. E. Kamentsev, V. Y. Shkuratov, Y. O. Kvashnin, C. Autieri, I. Di Marco, B. Sanyal, O. Eriksson, P. Nordblad and R. Mathieu, Polar Order and Frustrated Antiferromagnetism in Perovskite Pb2MnWO6 Single Crystals, *Inorg. Chem.*, 2016, **55**, 2791–2805.
44 R. Basnet, K. M. Kotur, M. Rybak, C. Stephenson, S. Bishop, C. Autieri, M. Birowska and J. Hu, Controlling magnetic exchange and anisotropy by nonmagnetic ligand substitution in layered mPX_3 (m = Ni, Mn; x = S, Se), *Phys. Rev. Res.*, 2022, **4**, 023256.
45 S. J. Youn, B. I. Min and A. J. Freeman, Crossroads electronic structure of MnS, MnSe, and MnTe, *Phys. Status Solidi B*, 2004, **241**, 1411–1414.
46 C. Autieri, C. Śliwa, R. Islam, G. Cuono and T. Dietl, Momentum-resolved spin splitting in Mn-doped trivial CdTe and topological HgTe semiconductors, *Phys. Rev. B*, 2021, **103**, 115209.
47 K. Harun, N. A. Salleh, B. Deghfel, M. K. Yaakob and A. A. Mohamad, DFT + U calculations for electronic, structural, and optical properties of ZnO wurtzite structure: A review, *Results Phys.*, 2020, **16**, 102829.

48 L.-D. Yuan, Z. Wang, J.-W. Luo, E. I. Rashba and A. Zunger, Giant momentum-dependent spin splitting in centrosymmetric low-Z antiferromagnets, *Phys. Rev. B*, 2020, **102**, 014422.
49 I. Turek, Altermagnetism and magnetic groups with pseudoscalar electron spin, *Phys. Rev. B*, 2022, **106**, 094432.
50 C. Autieri, R. M. Sattigeri, G. Cuono and A. Fakhredin, Dzyaloshinskii–Moriya interaction inducing weak ferromagnetism in centrosymmetric altermagnets and weak ferrimagnetism in noncentrosymmetric altermagnets, 2023, *arXiv*, preprint, arXiv:2312.07678, DOI: **10.48550/arxiv.org/abs/2312.07678**.
51 R. M. Sattigeri, G. Cuono and C. Autieri, Altermagnetic surface states: towards the observation and utilization of altermagnetism in thin films, interfaces and topological materials, *Nanoscale*, 2023, **15**, 16998–17005.
52 K. Momma and F. Izumi, VESTA 3 for three-dimensional visualization of crystal, volumetric and morphology data, *J. Appl. Crystallogr.*, 2011, **44**, 1272–1276.